

Supporting Information

Structural and Magnetic Properties of Tetragonal Perovskite $\text{BaFe}_{1-x}\text{Bi}_x\text{O}_{3-\delta}$

Muhammad Asim Farid,^a Hao Zhang,^a Xiaohuan Lin,^a Aimei Yang,^b Sihai Yang,^c Guobao Li,^{a*}
Fuhui Liao,^a Jianhua Lin^{a*}

^aBeijing National Laboratory for Molecular Sciences, State Key Laboratory of Rare Earth Materials Chemistry and Applications, College of Chemistry and Molecular Engineering, Peking University, Beijing 100871, P. R. China.

^bCollege of Materials and Engineering of Guangxi Guilin University of Technology, Guilin 541004, China.

^cSchool of Chemistry, University of Nottingham, University Park, Nottingham NG7 2RD, UK.

*To whom correspondence should be addressed, Email: liguobao@pku.edu.cn, and jhlin@pku.edu.cn; Tel: (8610)62750342, Fax: (8610)62753541.

Content

| | |
|--|----|
| 1. Choice of space group for refinement of BFB15 ($\text{BaFe}_{0.85}\text{Bi}_{0.15}\text{O}_{3-\delta}$)..... | 2 |
| 2. Chemical Analysis of BFB15 ($\text{BaFe}_{0.85}\text{Bi}_{0.15}\text{O}_{3-\delta}$) and BFB24 ($\text{BaFe}_{0.76}\text{Bi}_{0.24}\text{O}_{3-\delta}$)..... | 4 |
| 3. Rietveld Refinement Details of powder X-ray diffraction data collected at 300 K for $\text{BaFe}_{1-x}\text{Bi}_x\text{O}_{3-\delta}$ | 7 |
| 4. XPS analysis data of $\text{BaFe}_{1-x}\text{Bi}_x\text{O}_{3-\delta}$ | 11 |
| 5. Magnetic susceptibility χ and its inverse χ^{-1} verses temperature of $\text{BaFe}_{1-x}\text{Bi}_x\text{O}_{3-\delta}$ | 18 |
| 6. The ^{57}Fe Mössbauer spectra of BFB15 ($\text{BaFe}_{0.85}\text{Bi}_{0.15}\text{O}_{3-\delta}$)..... | 21 |
| 7. Rietveld Refinement Details of the neutron diffraction data collected at 3K and 55K for BFB15 ($\text{BaFe}_{0.85}\text{Bi}_{0.15}\text{O}_{3-\delta}$)..... | 21 |

1. The choice of space group for the refinement of $\text{BaFe}_{1-x}\text{Bi}_x\text{O}_{3-\delta}$

The powder X-ray, synchrotron and neutron diffraction data of BFB15 ($\text{BaFe}_{0.85}\text{Bi}_{0.15}\text{O}_{3-\delta}$) can be fitted well with space group $Pm3m$ as reported for C- BaFeO_3 .¹ The refinement plots are shown in Figure S1 and the details are listed in Table S1. However careful refinement shows that the high resolution synchrotron powder diffraction data are also fitted well with space group $P4/mmm$ (model 2) : three peaks are found around 62.26° (Figure S1d), but only one peak is expected by the space group $Pm3m$. Therefore, the space group $P4/mmm$ is chosen to describe the structure of BFB3 instead of the space group $Pm3m$ for C- BaFeO_3 .

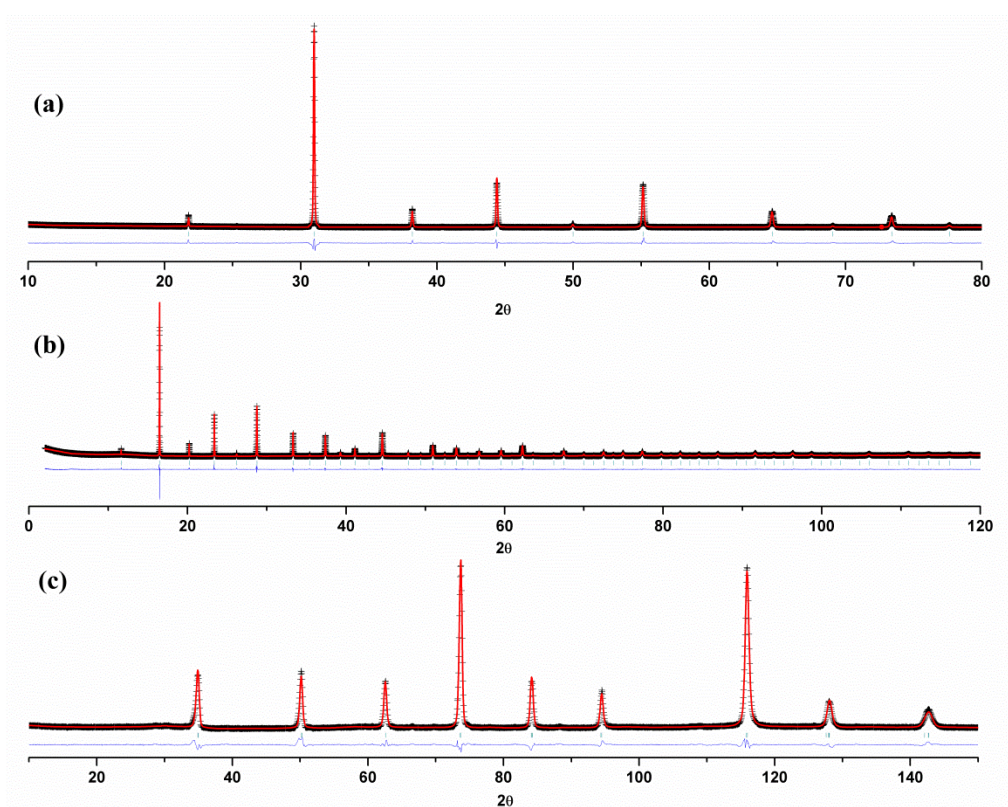


Fig. S1 Rietveld plots of powder X-ray (a), Synchrotron (b) and neutron (c) powder diffraction pattern diffraction pattern of BFB15($\text{BaFe}_{0.85}\text{Bi}_{0.15}\text{O}_{3-\delta}$) in space group $Pm3m$. The symbol + represents the observed value, solid line represents the calculated value; the marks below the diffraction patterns are the calculated reflection positions, and the difference curve is shown at the bottom of the Figure.

Table S1 Rietveld Refinement Details of BFB15 ($\text{BaFe}_{0.85}\text{Bi}_{0.15}\text{O}_{3-\delta}$) with space group $Pm3m$ (model 1).

| Lattice parameters | | $a = 4.0759(1) \text{ \AA}$ | |
|-----------------------|--|-----------------------------|------------------|
| Atom | (x,y,z) | Occupancy | U_{iso} |
| Ba1 | 0.0000, 0.0000, 0.0000 | 1.00 | 0.0028 |
| Fe1 | 0.5000, 0.5000, 0.5000 | 0.85(1) | 0.0073 |
| Bi1 | 0.5000, 0.5000, 0.5000 | 0.15(1) | 0.0073 |
| O1 | 0.5000, 0.5000, 0.0000 | 3.00(1) | 0.0052 |
| R factor ^a | $R_{\text{wp}}^{\text{x}} = 0.046$, $R_{\text{p}}^{\text{x}} = 0.031$; $R_{\text{wp}}^{\text{s}} = 0.064$, $R_{\text{p}}^{\text{s}} = 0.050$; $R_{\text{wp}}^{\text{n}} = 0.066$, $R_{\text{p}}^{\text{n}} = 0.044$ | | |

[a] R_{wp}^{x} , R_{p}^{x} are the R factor of the whole patterns and the peaks only for X-ray diffraction data, respectively; R_{wp}^{s} , R_{p}^{s} are the R factor of the whole patterns and the peaks only for synchrotron diffraction data, respectively; R_{wp}^{n} , R_{p}^{n} are the R factor of the whole patterns and the peaks only for neutron diffraction data, respectively.

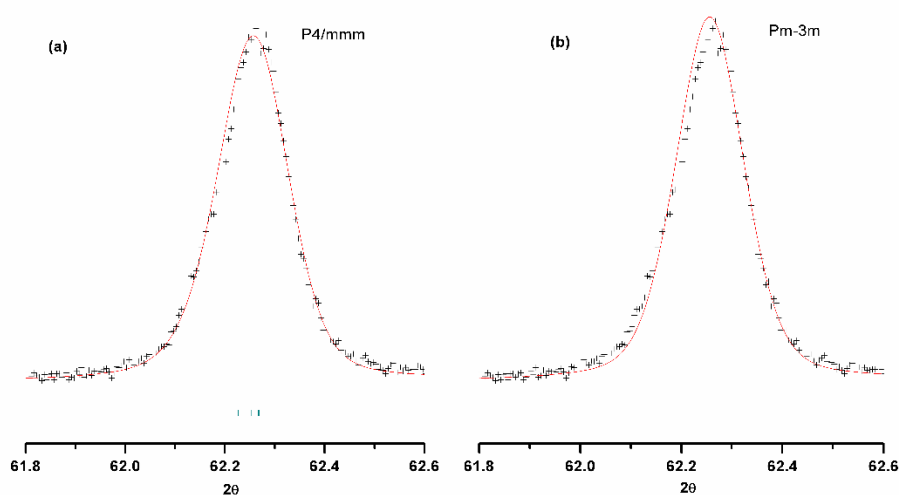


Fig. S1d Rietveld plots of Synchrotron powder diffraction pattern of BFB15 ($\text{BaFe}_{0.85}\text{Bi}_{0.15}\text{O}_{3-\delta}$) from 61.8° to 62.6° 2 theta degree value with space group $P4/mmm$ (a) and $Pm3m$ (b)

2. About the composition of $\text{BaFe}_{1-x}\text{Bi}_x\text{O}_3$

We used chemical titration to analyze the composition of the samples BFB15 ($\text{BaFe}_{1-x}\text{Bi}_x\text{O}_{3-\delta}$, $x = 0.15$) and BFB24 ($\text{BaFe}_{1-x}\text{Bi}_x\text{O}_{3-\delta}$, $x = 0.24$).

a) Complex titration of BFB15 ($\text{BaFe}_{1-x}\text{Bi}_x\text{O}_{3-\delta}$, $x = 0.15$) for Fe and Bi

3.000 g of BFB15 sample was solved in concentrated nitric acid. The solution was transferred to a 250ml volumetric flask and diluted to 250.0ml with dilute nitric acid.

Ethylenediaminetetraacetic acid (EDTA) with the concentration of 0.02500mol/L was used as titrant. The pH value of the solution was monitored by a PHS-3B type of pH meter, and controlled to about 1.0 by adding several drops of dilute nitric acid or concentrated nitric acid to titrate Bi^{3+} with two drops of xylenol orange (0.2% ethanol solution) as indicator at room temperature, or controlled to about 2.0 to titrate both Bi^{3+} and Fe^{3+} with 2.0ml 15% Sulfosalicylic acid solution as indicator at about 60°C. The results are shown in **Table S2a**, from which it is known that there are about 0.001705(1) mol of Bi and 0.009621(1) mol of Fe in the sample.

Table S2a. The details of the complex titration of Bi^{3+} and Fe^{3+} for compound BFB15 ($\text{BaFe}_{1-x}\text{Bi}_x\text{O}_{3-\delta}$, $x = 0.15$).

| Flask | Volume of solution (ml) | Volume of the EDTA for the titration of Bi^{3+} (ml) | Volume of the EDTA for the titration of Bi^{3+} (ml) and Fe^{3+} |
|-------|-------------------------|---|--|
| 1 | 25.00ml | 6.82ml | 45.33 ml |
| 2 | 25.00ml | 6.81 ml | 45.30 ml |
| 3 | 25.00ml | 6.84 ml | 45.32 ml |

Then 3g of the compound BFB15 ($\text{BaFe}_{1-x}\text{Bi}_x\text{O}_{3-\delta}$, $x = 0.15$) contains

$$\text{Bi} = 0.001705(1) \text{ mole}$$

$$\text{Fe} = 0.009621(1) \text{ mole}$$

b) BaSO_4 gravimetry to determine the content of Ba in the compound

1.000 g of BFB15 was added into a 250ml beaker, solved in the solution of 8ml HCl (2 mol/L), 1ml H_2O_2 (30%, A. R.) and 30ml distilled water at about 70°C, and diluted to 70ml. The solution was then kept at 70°C on a water bath during the adding drop by drop of 0.08mol/L H_2SO_4 . After the precipitation of BaSO_4 was completed and aging for 10 hours, the precipitate was washed by 0.01 mol/L H_2SO_4 , distilled water respectively and filtered with quantitative filter paper. The temperatures for ashing and constant weight were 300 and 800°C, respectively. The corresponding data were listed in Table S2b.

Table S2b. The details for BaSO_4 gravimetry to determine the content of Ba in the compound

| Flask | Weight of the sample (g) | Weight of the precipitate (g) | Weight of the Ba in 1 g of sample |
|---------|--------------------------|-------------------------------|-----------------------------------|
| 1 | 1.000g | 0.8772g | 0.5162g |
| 2 | 1.000g | 0.8740g | 0.5143g |
| 3 | 1.000g | 0.8779g | 0.5166g |
| average | | | 0.5157 |

Then 3g of the compound BFB15 ($\text{BaFe}_{1-x}\text{Bi}_x\text{O}_{3-\delta}$, $x = 0.15$) contains $\text{Ba} = 0.5157 \times 3 = 1.5471\text{g}$

$$\text{No. of moles of Ba in 3g of BFB15} = 1.5471/137.34 = 0.01126\text{mole}$$

c) The composition of the compound BFB15 ($\text{BaFe}_{1-x}\text{Bi}_x\text{O}_{3-\delta}$, $x = 0.15$)

From the above results, one can obtain mole ratio of elements in compound

$$\text{Ba:Fe:Bi} = 0.01126: 0.009621: 0.001705 = = 99.3:84.7:15.03$$

Then the formula of BFB15 was noted as $(\text{BaFe}_{0.85}\text{Bi}_{0.15}\text{O}_{3-\delta})$

We used same chemical titration method to analyze the composition of sample BFB24 ($\text{BaFe}_{1-x}\text{Bi}_x\text{O}_{3-\delta}$, $x = 0.24$). The composition of the compound from the titration analysis was found to be

3 g of BFB24 contains

No. of moles of Fe = 0.008153

No. of moles of Bi = 0.002575

No. of moles of Ba = 0.01074

Mole ratio of Ba, Fe and Bi.

Ba:Fe:Bi = Ba:Fe:Bi = 0.01074: 0.008153: 0.002575 = 100.1:75.98:24.0

Then the formula of BFB24 was noted as $(\text{BaFe}_{0.76}\text{Bi}_{0.24}\text{O}_{3-\delta})$

So the final results of chemical titrations confirm the composition of BFB15 as $\text{BaFe}_{0.85}\text{Bi}_{0.15}\text{O}_{3-\delta}$ and BFB24 as $\text{BaFe}_{0.76}\text{Bi}_{0.24}\text{O}_{3-\delta}$ considering the analysis error.

d) The determination of the oxygen content

The TGA analysis has been performed for the sample BFB9 ($\text{BaFe}_{1-x}\text{Bi}_x\text{O}_{3-\delta}$, $x = 0.09$). The corresponding data is shown below.

Hydrogen-reduction thermogravimetry was used to try to determine the oxygen content of BFB9 ($\text{BaFe}_{1-x}\text{Bi}_x\text{O}_{3-\delta}$, $x = 0.09$). A small sample of powder (about 20 mg) was placed in an alumina crucible in a Netzsch STA 449C thermogravimetric analyzer and heated at $10^\circ\text{C min}^{-1}$ in a flowing 5% H_2 /95%Ar atmosphere from room temperature to 800°C . BaO, Bi_2O_3 and $\text{Ba}_2\text{Fe}_2\text{O}_5$ were identified by XRD of the final products of the reduction process as shown in Figure S2a. Then one can calculate the expected mass loss for BFB9. If $\delta \approx 0.00$, then the expected mass loss is 3.14%. However, the obtained data shown in Figure S2b indicated that the mass loss was larger than 3.14%. If one considers that there is some oxygen vacancy in $\text{Ba}_2\text{Fe}_2\text{O}_{5-x}$, then at the maximum value of $x=1$, the expected mass loss is about 6.00%, which may be agreeable to 6.13% shown in the Figure S2b. However, it is not easy to accept that $\text{Ba}_2\text{Fe}_2\text{O}_{5-x}$ can be $\text{Ba}_2\text{Fe}_2\text{O}_4$ without structure change. In addition, around the mass loss of about 6.13% there is not platform. It is very difficult to have an acceptable data to assess the value of Oxygen in the compound of $\text{BaFe}_{1-x}\text{Bi}_x\text{O}_{3-\delta}$. The loss of about 6.13% or more may be attributed to the leave of Bi_2O_3 when the temperature is higher than 600°C with the flowing of gas. Therefore, we think that the TGA method we used could not give a clear answer about the O-content of our samples.

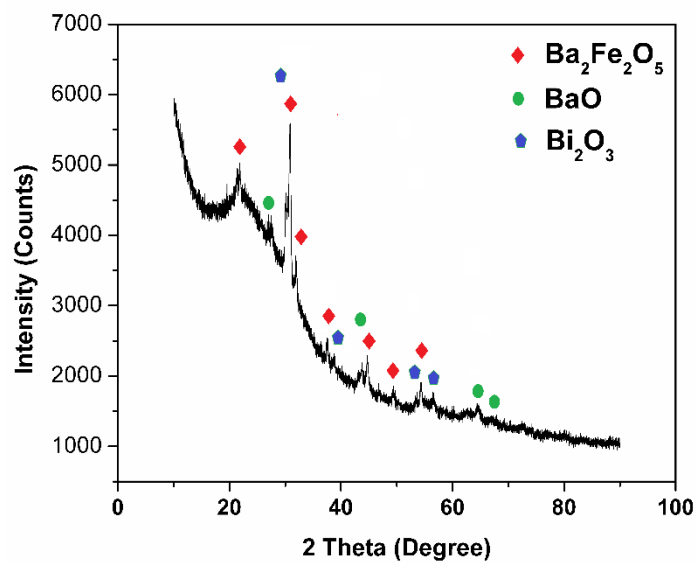


Figure S2a XRD pattern of final products of the reduction process of BFB9 in a flowing 5% H_2 /95% Ar atmosphere.

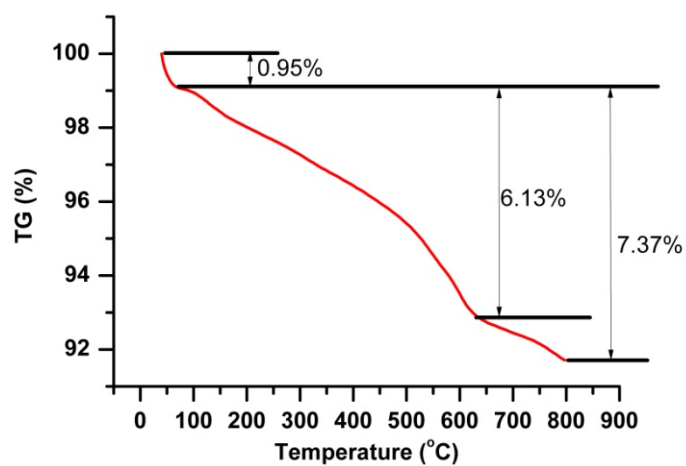


Figure S2b TG curve for the reduction of BFB9 in a flowing 5% H_2 /95% Ar atmosphere. The mass loss about 0.95% before 100°C is typically due to the moisture and/or CO_2 adhered to the sample.

3. The refinement details of the Powder X-ray diffraction data collected at 300 K for the $\text{BaFe}_{1-x}\text{Bi}_x\text{O}_{3-\delta}$ series.

The Powder X-ray diffraction data collected at 300K for the $\text{BaFe}_{1-x}\text{Bi}_x\text{O}_{3-\delta}$ series are refined using GSAS software.²⁻³ to obtain the lattice parameters and atoms coordinates of the nuclear structure with the refinement details listed in Table S3. The corresponding Rietveld plots are shown in Fig.S2a to S2h. Rietveld plots of Powder X-ray diffraction (PXRD) data were collected on a PANalytical Empyrean diffractometer with Cu $K_{\alpha 1}$ radiation (1.540598 Å) at 50 kV and 40 mA.

Table S3. Rietveld Refinement Details of $\text{BaFe}_{1-x}\text{Bi}_x\text{O}_{3-\delta}$ in space group P4/mmm using GSAS software

| $\text{BaFe}_{1-x}\text{Bi}_x\text{O}_{3-\delta}$ | | X = 0.09 | X = 0.12 | X = 0.18 | X = 0.21 | X = 0.24 | X = 0.27 | X = 0.30 | X = 0.35 |
|---|----------|---------------------------------|---------------------------------|---------------------------------|---------------------------------|---------------------------------|---------------------------------|---------------------------------|---------------------------------|
| Lattice params | a (Å) | 4.0672(1) | 4.0720(1) | 4.0801(1) | 4.0842(1) | 4.0883(1) | 4.0927(1) | 4.0965(1) | 4.1001(1) |
| | c (Å) | 4.0684(1) | 4.0732(1) | 4.0826(1) | 4.0860(1) | 4.0904(1) | 4.0935(1) | 4.0999(1) | 4.1091(1) |
| Volume (Å ³) | | 67.300(1) | 67.540(1) | 67.962(1) | 68.156(1) | 68.368(1) | 68.569(1) | 68.802(1) | 69.078(1) |
| Atom | | (x,y,z) |
| Ba1 | | 0.00000, 0.00000, 0.00000 |
| Fe1 | | 0.50000, 0.50000, 0.50000 |
| Bi1 | | 0.50000, 0.50000, 0.50000 |
| O1 | | 0.50000, 0.50000, 0.00000 |
| O2 | | 0.50000, 0.00000, 0.50000 |
| R | R_{wp} | 0.0512 | 0.0468 | 0.0522 | 0.0476 | 0.0648 | 0.0609 | 0.0668 | 0.062 |

| factor ^c | R_p | 0.0299 | 0.0319 | 0.0340 | 0.0309 | 0.0374 | 0.0366 | 0.0409 | 0.034 |
|---------------------|-------|--------|--------|--------|--------|--------|--------|--------|-------|
|---------------------|-------|--------|--------|--------|--------|--------|--------|--------|-------|

^c R_{wp}^x , R_p^x are the R factors of the whole patterns and the peaks only for X-ray diffraction data, respectively.

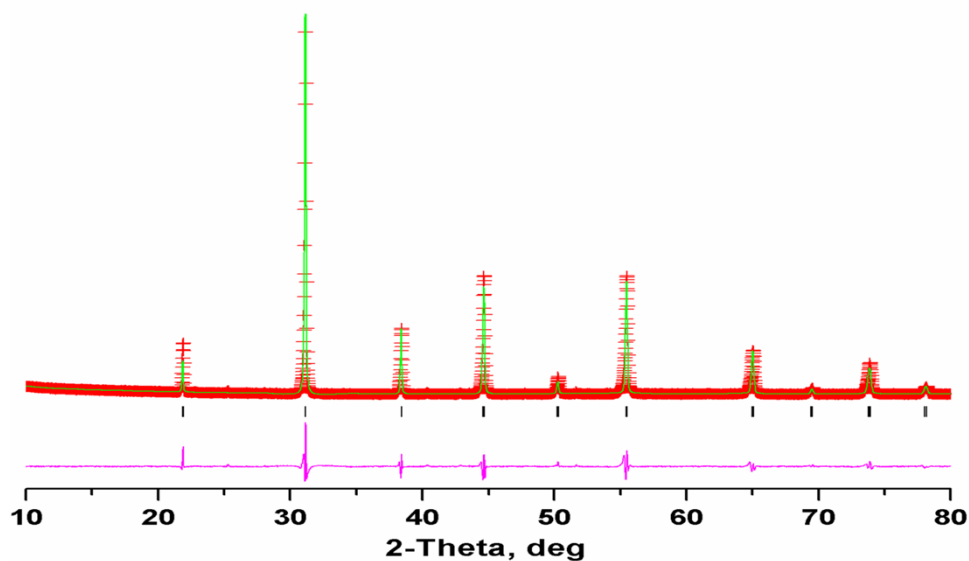


Figure S3a. Rietveld plot of powder X-ray diffraction pattern of $BaFe_{0.91}Bi_{0.09}O_{3-\delta}$. The symbol + represents the observed value, solid line represents the calculated value; the marks below the diffraction patterns are the calculated reflection positions, and the difference curve is shown at the bottom of the Figure.

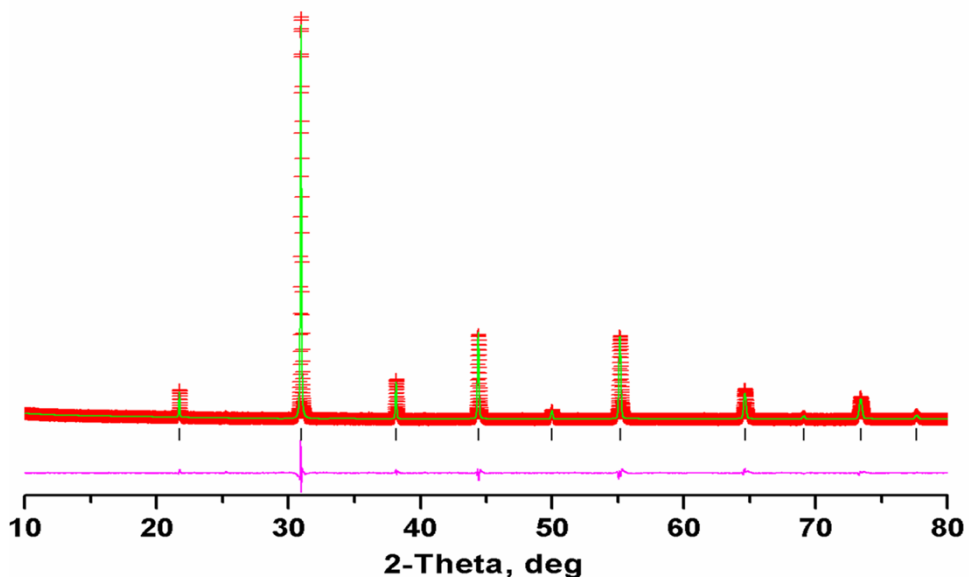


Figure S3b. Rietveld plots of powder X-ray diffraction pattern of $BaFe_{0.88}Bi_{0.12}O_{3-\delta}$. The symbol + represents the observed value, solid line represents the calculated value; the marks below the diffraction patterns are the calculated reflection positions, and the difference curve is shown at the bottom of the Figure.

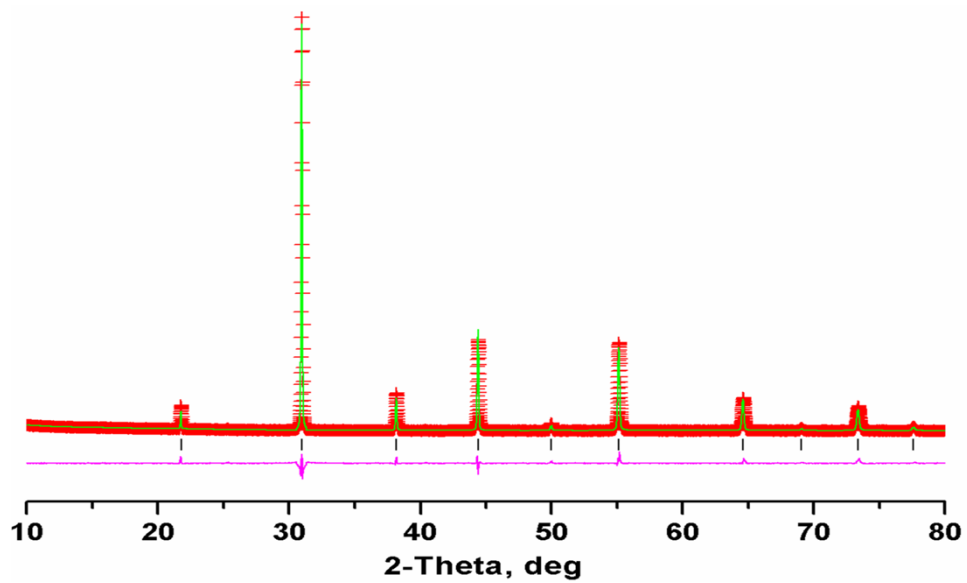


Figure S3c. Rietveld plots of powder X-ray diffraction pattern of $\text{BaFe}_{0.85}\text{Bi}_{0.15}\text{O}_{3-\delta}$. The symbol + represents the observed value, solid line represents the calculated value; the marks below the diffraction patterns are the calculated reflection positions, and the difference curve is shown at the bottom of the Figure.

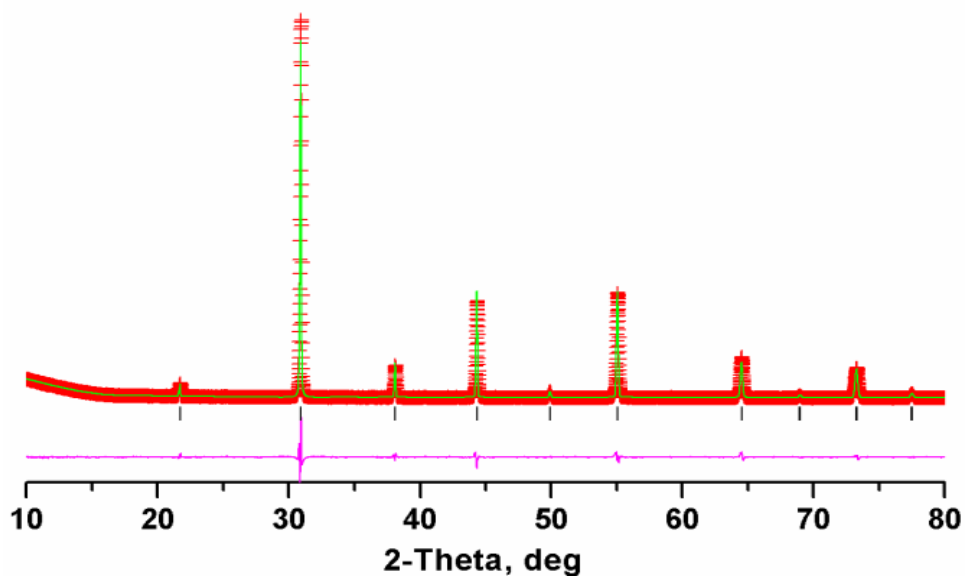


Figure S3d. Rietveld plots of powder X-ray diffraction pattern of $\text{BaFe}_{0.82}\text{Bi}_{0.18}\text{O}_{3-\delta}$. The symbol + represents the observed value, solid line represents the calculated value; the marks below the diffraction patterns are the calculated reflection positions, and the difference curve is shown at the bottom of the Figure.

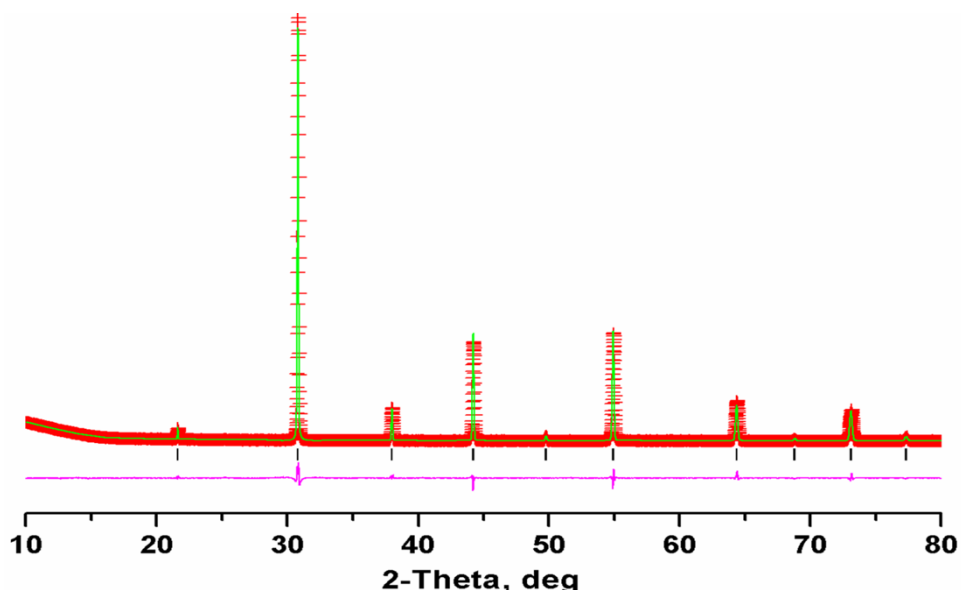


Figure S3e. Rietveld plots of powder X-ray diffraction pattern of $\text{BaFe}_{0.79}\text{Bi}_{0.21}\text{O}_{3-\delta}$. The symbol + represents the observed value, solid line represents the calculated value; the marks below the diffraction patterns are the calculated reflection positions, and the difference curve is shown at the bottom of the Figure.

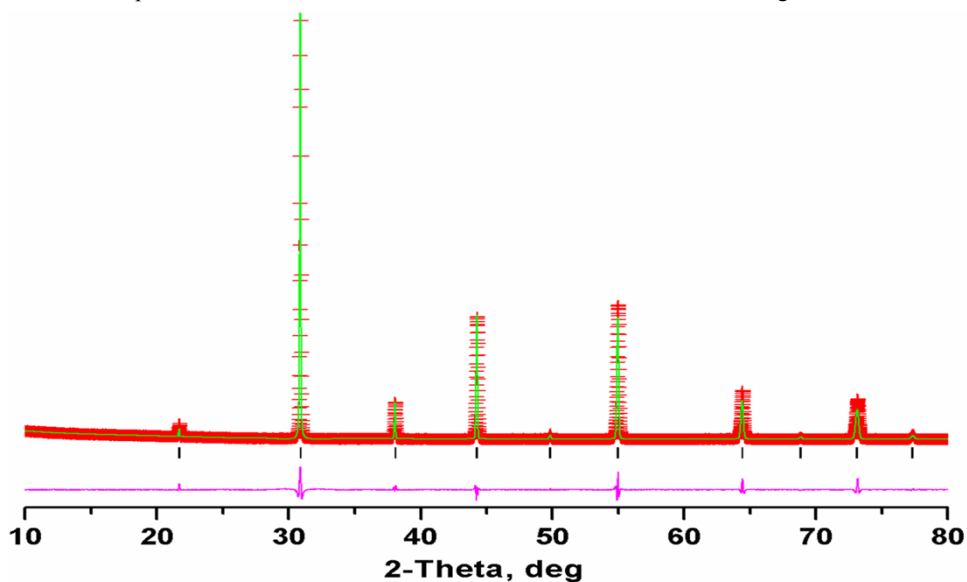


Figure S3f. Rietveld plots of powder X-ray diffraction pattern of $\text{BaFe}_{0.76}\text{Bi}_{0.24}\text{O}_{3-\delta}$. The symbol + represents the observed value, solid line represents the calculated value; the marks below the diffraction patterns are the calculated reflection positions, and the difference curve is shown at the bottom of the Figure.

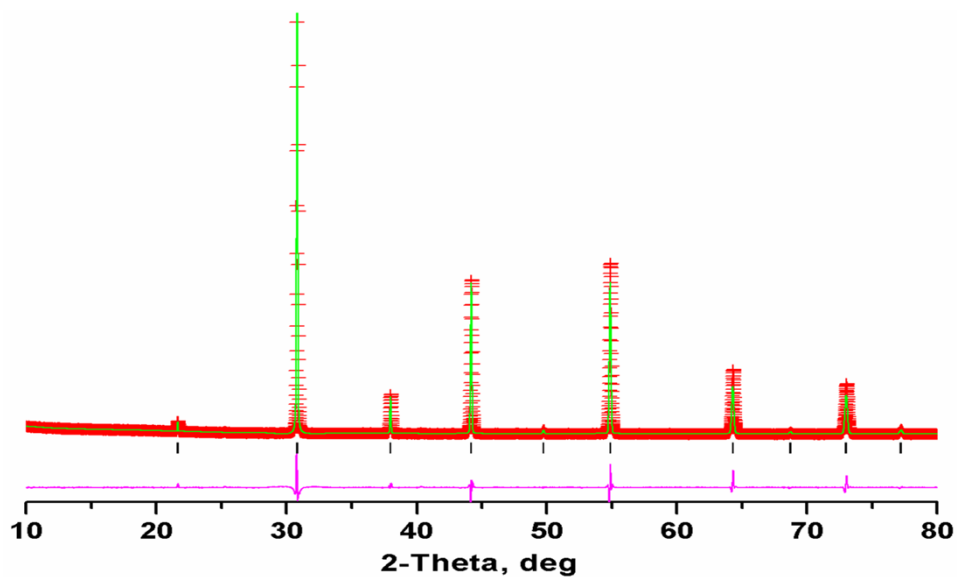


Figure S3g. Rietveld plots of powder X-ray diffraction pattern of $\text{BaFe}_{0.73}\text{Bi}_{0.27}\text{O}_{3-\delta}$. The symbol + represents the observed value, solid line represents the calculated value; the marks below the diffraction patterns are the calculated reflection positions, and the difference curve is shown at the bottom of the Figure.

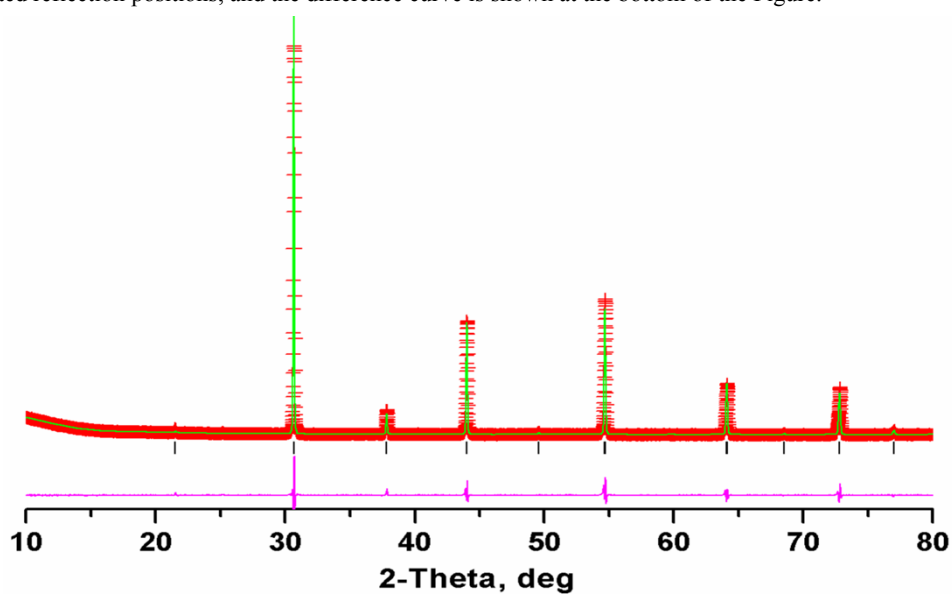


Figure S3h. Rietveld plots of powder X-ray diffraction pattern of $\text{BaFe}_{0.70}\text{Bi}_{0.30}\text{O}_{3-\delta}$. The symbol + represents the observed value, solid line represents the calculated value; the marks below the diffraction patterns are the calculated reflection positions, and the difference curve is shown at the bottom of the Figure.

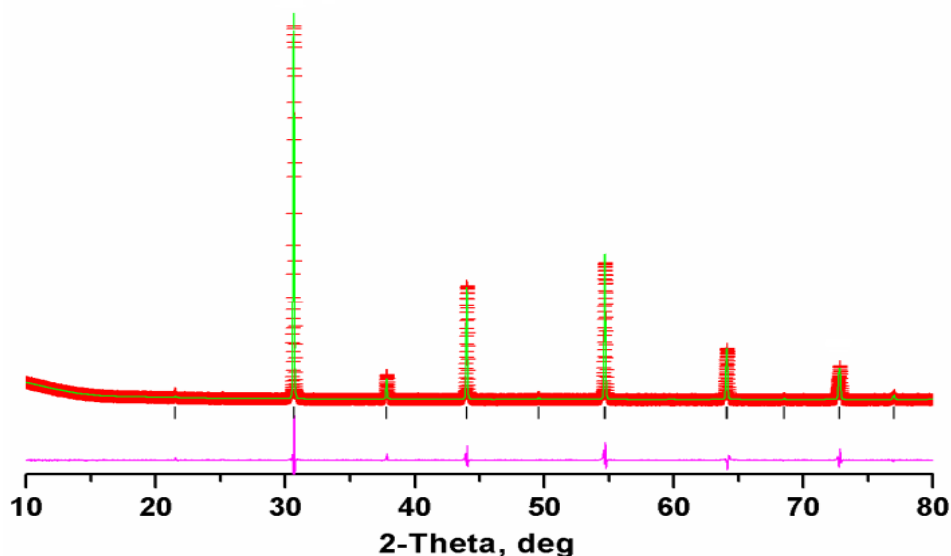


Figure S3i. Rietveld plots of powder X-ray diffraction pattern of $\text{BaFe}_{0.65}\text{Bi}_{0.35}\text{O}_{3-\delta}$. The symbol + represents the observed value, solid line represents the calculated value; the marks below the diffraction patterns are the calculated reflection positions, and the difference curve is shown at the bottom of the Figure.

4. XPS analysis data of $\text{BaFe}_{1-x}\text{Bi}_x\text{O}_{3-\delta}$ ($0.09 < x < 0.35$).

The X-ray photoelectron spectroscopy (XPS) patterns were acquired with a UK Kratos Axis Ultra spectrometer with Al $K\alpha$ X-ray source operated at 15 kV, 15 mA. The chamber pressure was less than 5.0×10^{-9} Torr. Electron binding energies were calibrated against the C 1s emission at $E_b = 284.8$ eV.

The C 1s core level for both of the samples displays two component peaks. First peak is doublet at 284.80 eV and 285.85-285.72 eV which belongs to carbon contamination⁴⁻⁵ and second peak is at around 289.19 and 289.13 eV which belongs to typical carbonate structures.⁶ The O 1s and Ba $3d_{5/2}$ also supports these results. The major O 1s peak in the range of 529.7 eV is characteristic peak for O^{2-} while Ba $3d_{5/2}$ peaks are fitted to doublets. This indicates the peaks near 778.30 eV originate from perovskite Ba ions while the second peak is characteristic of BaCO_3 ⁷.

Table S4. Binding Energies (eV) of C 1s, O 1s, Ba 3d_{5/2} Fe 2p_{3/2} and Bi 4f_{7/2} core levels for the series BaFe_{1-x}Bi_xO_{3-δ} (0.09<x<0.35).

| Sample | C 1s | O 1s | Fe2p _{3/2} | Bi 4f _{7/2} | Ba3d _{7/2} |
|--|--------|--------|---------------------|----------------------|---------------------|
| BaFe _{0.91} Bi _{0.09} O _{3-δ} | 284.80 | 528.73 | 709.99 | 157.86 | 778.67 |
| | 285.72 | 529.39 | 710.59 | 158.59 | 779.67 |
| | 289.19 | 530.99 | 718.02 | | |
| BaFe _{0.88} Bi _{0.12} O _{3-δ} | 284.80 | 528.49 | 709.93 | 157.94 | 778.33 |
| | 285.94 | 529.41 | 710.68 | 158.75 | 779.44 |
| | 289.07 | 530.91 | 718.09 | | |
| BaFe _{0.85} Bi _{0.15} O _{3-δ} | 284.80 | 528.45 | 709.84 | 157.83 | 778.32 |
| | 285.85 | 529.03 | 710.54 | 158.65 | 779.61 |
| | 289.19 | 531.06 | 718.04 | | |
| BaFe _{0.88} Bi _{0.18} O _{3-δ} | 284.80 | 528.52 | 709.79 | 158.01 | 778.33 |
| | 285.85 | 529.29 | 710.47 | 158.85 | 779.63 |
| | 289.08 | 531.00 | 718.27 | | |
| BaFe _{0.79} Bi _{0.21} O _{3-δ} | 284.80 | 528.42 | 709.98 | 157.85 | 778.34 |
| | 285.70 | 528.97 | 710.88 | 158.51 | 779.68 |
| | 289.08 | 531.02 | 718.39 | | |
| BaFe _{0.76} Bi _{0.24} O _{3-δ} | 284.80 | 528.59 | 709.76 | 157.89 | 778.39 |
| | 285.72 | 529.70 | 710.92 | 158.74 | 779.69 |
| | 289.13 | 531.01 | 718.02 | | |
| BaFe _{0.73} Bi _{0.27} O _{3-δ} | 284.80 | 528.64 | 709.73 | 157.91 | 778.14 |
| | 285.72 | 529.13 | 710.78 | 158.52 | 779.72 |
| | 289.16 | 530.90 | 718.07 | | |
| BaFe _{0.70} Bi _{0.30} O _{3-δ} | 284.80 | 528.60 | 709.71 | 158.02 | 778.34 |
| | 285.72 | 529.10 | 710.83 | 158.68 | 779.77 |
| | 289.19 | 530.95 | 717.73 | | |
| BaFe _{0.65} Bi _{0.35} O _{3-δ} | 284.80 | 528.65 | 709.63 | 157.88 | 778.51 |
| | 285.62 | 529.38 | 710.90 | 158.62 | 779.82 |
| | 289.15 | 531.20 | 718.01 | | |

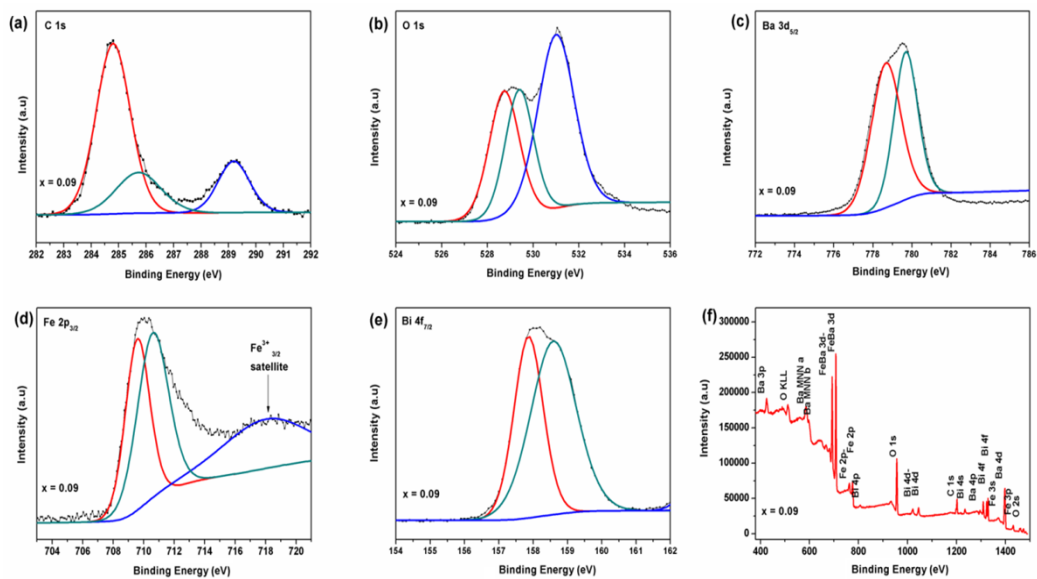


Figure S4a. XPS spectra of C 1s (a), O 1s (b), Ba 3d_{5/2} (c), Fe 2p_{3/2} (d), Bi 4f_{7/2} (e) and $\text{BaFe}_{0.91}\text{Bi}_{0.09}\text{O}_{3-\delta}$ (f)

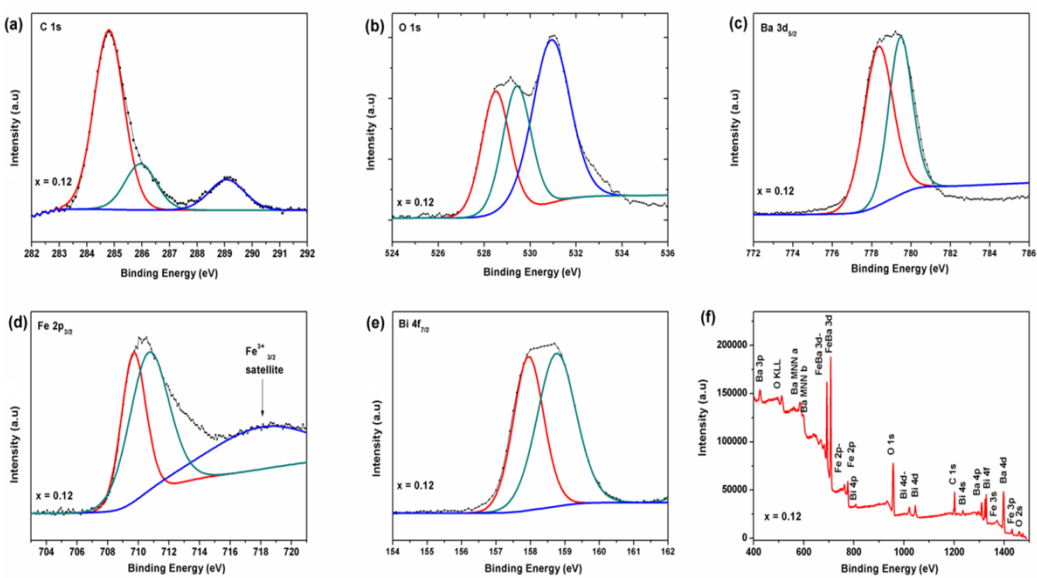


Figure S4b. XPS spectra of C 1s (a), O 1s (b), Ba 3d_{5/2} (c), Fe 2p_{3/2} (d), Bi 4f_{7/2} (e) and $\text{BaFe}_{0.88}\text{Bi}_{0.12}\text{O}_{3-\delta}$ (f)

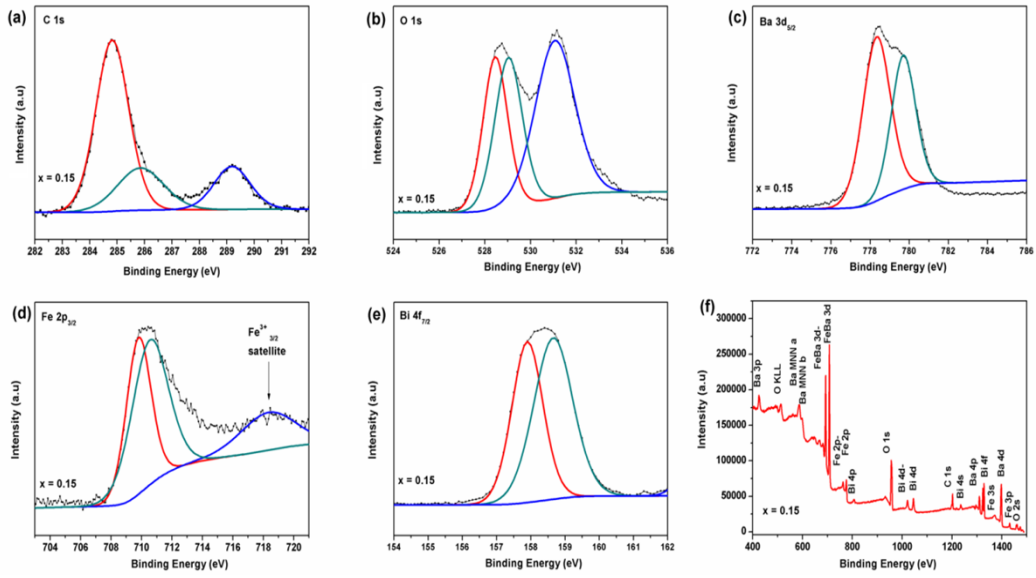


Figure S4c. XPS spectra of C 1s (a), O 1s (b), Ba 3d_{5/2} (c), Fe 2p_{3/2} (d), Bi 4f_{7/2} (e) and BaFe_{0.85}Bi_{0.15}O_{3-δ} (f)

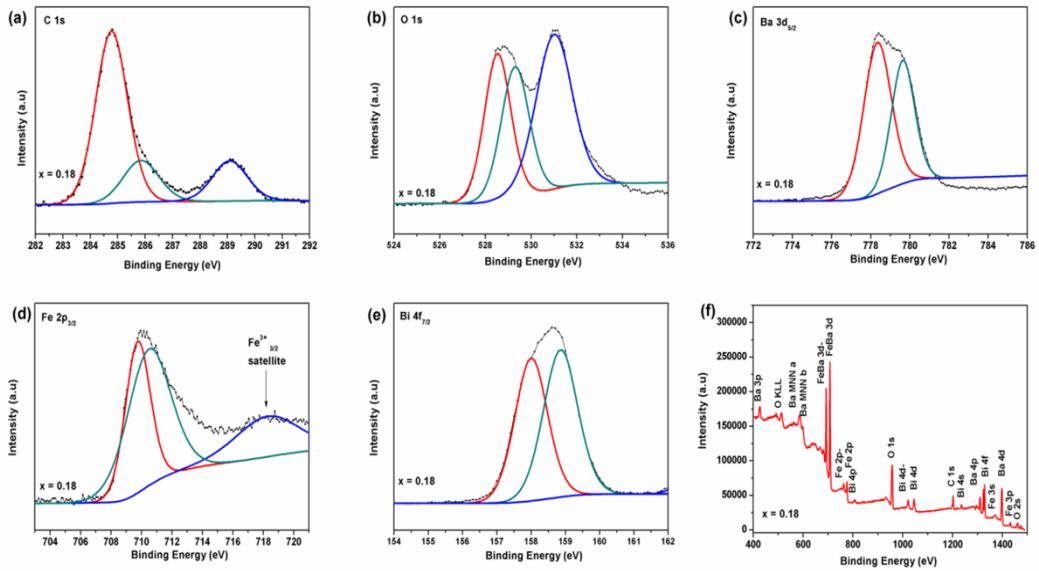


Figure S4d. XPS spectra of C 1s (a), O 1s (b), Ba 3d_{5/2} (c), Fe 2p_{3/2} (d), Bi 4f_{7/2} (e) and BaFe_{0.82}Bi_{0.18}O_{3-δ} (f)

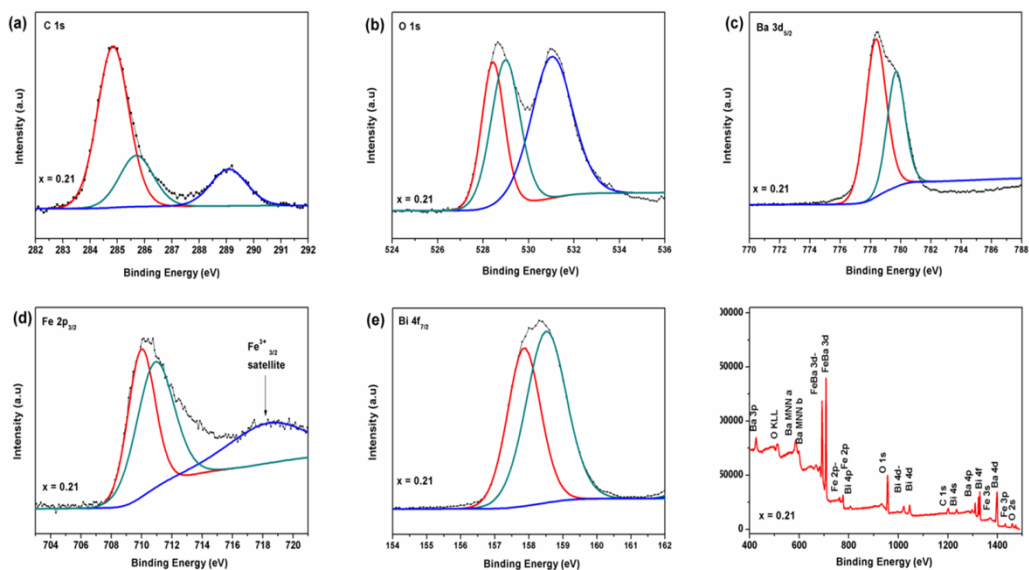


Figure S4e. XPS spectra of C 1s (a), O 1s (b), Ba 3d_{5/2} (c), Fe 2p_{3/2} (d), Bi 4f_{7/2} (e) and BaFe_{0.79}Bi_{0.21}O_{3-δ} (f)

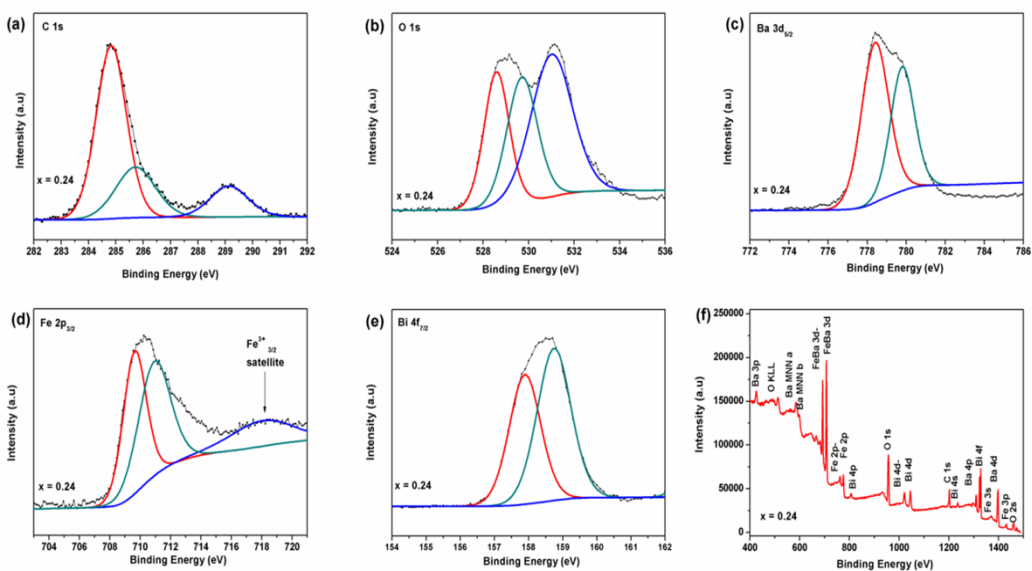


Figure S4f. XPS spectra of C 1s (a), O 1s (b), Ba 3d_{5/2} (c), Fe 2p_{3/2} (d), Bi 4f_{7/2} (e) and BaFe_{0.76}Bi_{0.24}O_{3-δ} (f)

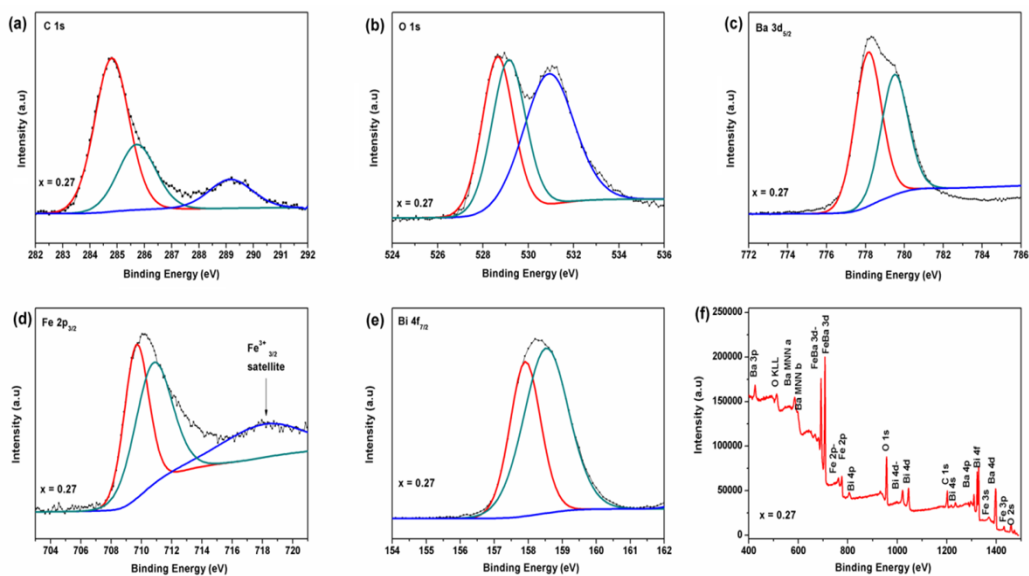


Figure S4g. XPS spectra of C 1s (a), O 1s (b), Ba 3d_{5/2} (c), Fe 2p_{3/2} (d), Bi 4f_{7/2} (e) and BaFe_{0.73}Bi_{0.27}O_{3-δ} (f)

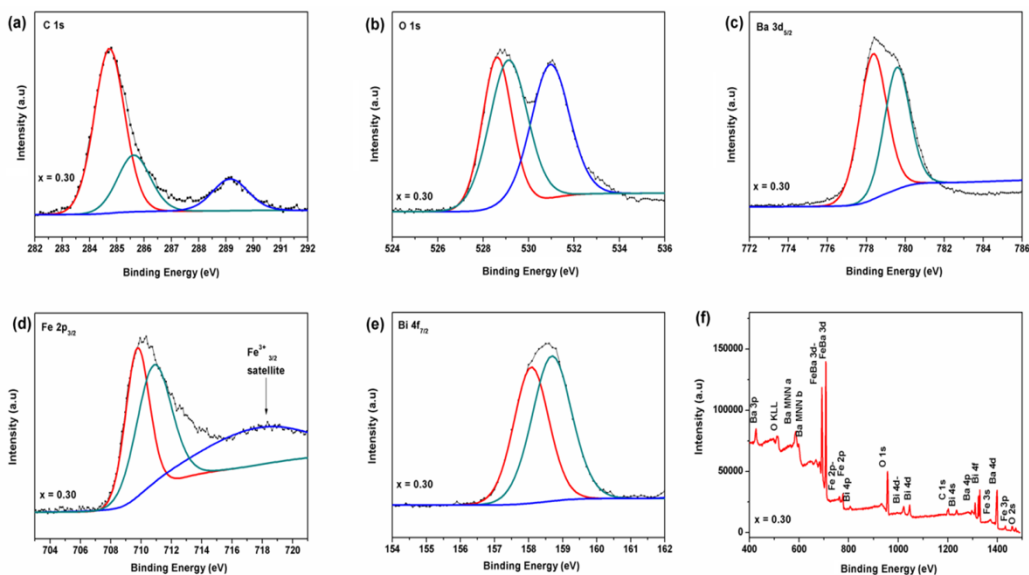


Figure S4h. XPS spectra of C 1s (a), O 1s (b), Ba 3d_{5/2} (c), Fe 2p_{3/2} (d), Bi 4f_{7/2} (e) and BaFe_{0.70}Bi_{0.30}O_{3-δ} (f)

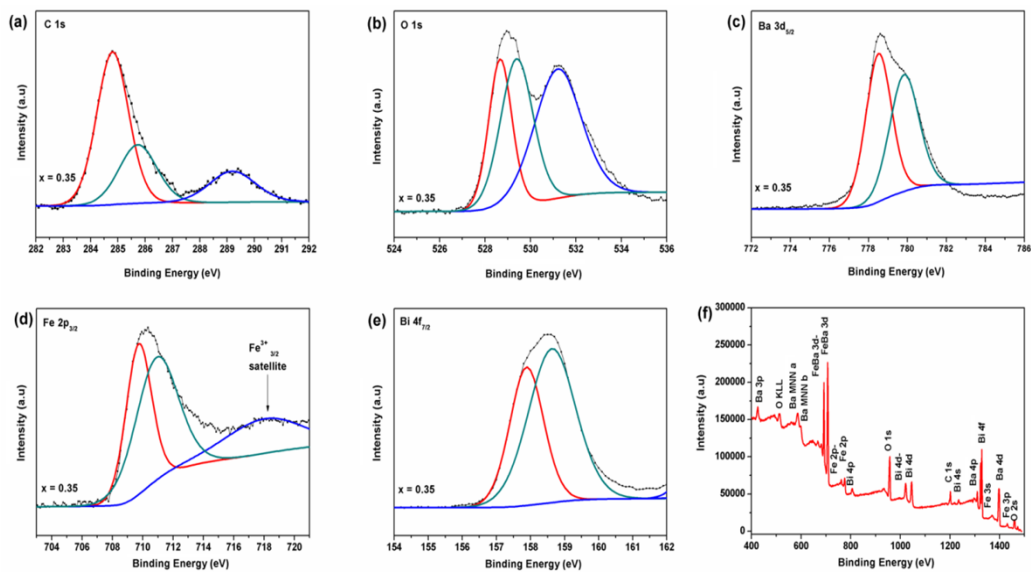


Figure S4i. XPS spectra of C 1s (a), O 1s (b), Ba 3d_{5/2} (c), Fe 2p_{3/2} (d), Bi 4f_{7/2} (e) and BaFe_{0.65}Bi_{0.35}O_{3-δ} (f)

5. Magnetic susceptibility χ and its inverse χ^{-1} verses temperature of BaFe_{1-x}Bi_xO_{3-δ} (0.09 < x < 0.35).

The magnetic properties were investigated with a Quantum design physical property measurement system (PPMS) from 5 K to 300 K.

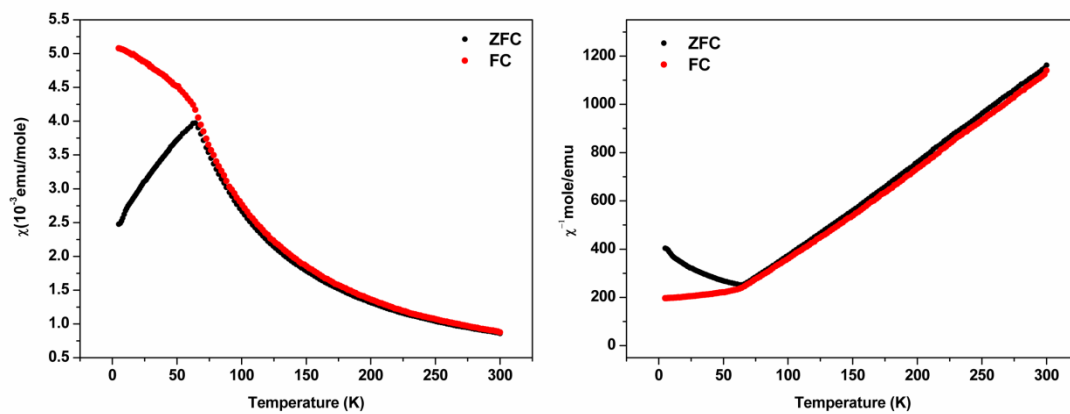


Figure S5a. Molar magnetic susceptibility χ and inverse molar magnetic susceptibility χ^{-1} vs temperature of BaFe_{0.91}Bi_{0.09}O_{3-δ}

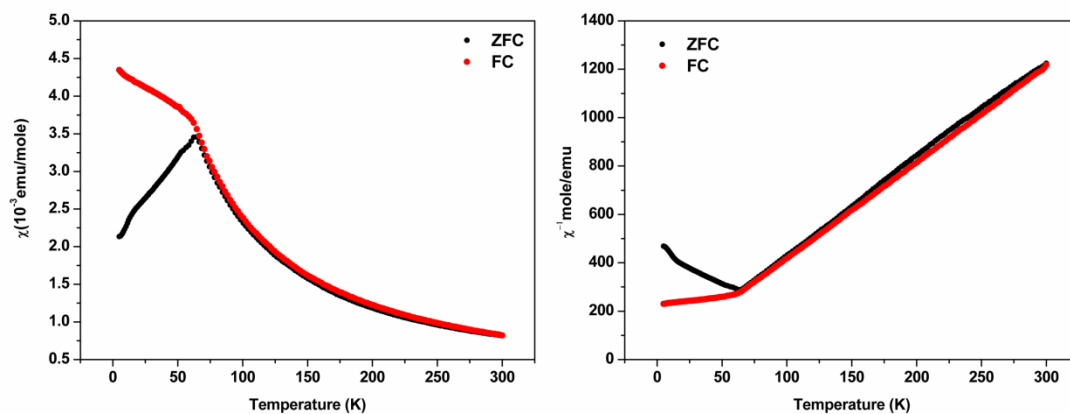


Figure S5b. Molar magnetic susceptibility χ and inverse molar magnetic susceptibility χ^{-1} vs temperature of $\text{BaFe}_{0.88}\text{Bi}_{0.12}\text{O}_{3-\delta}$

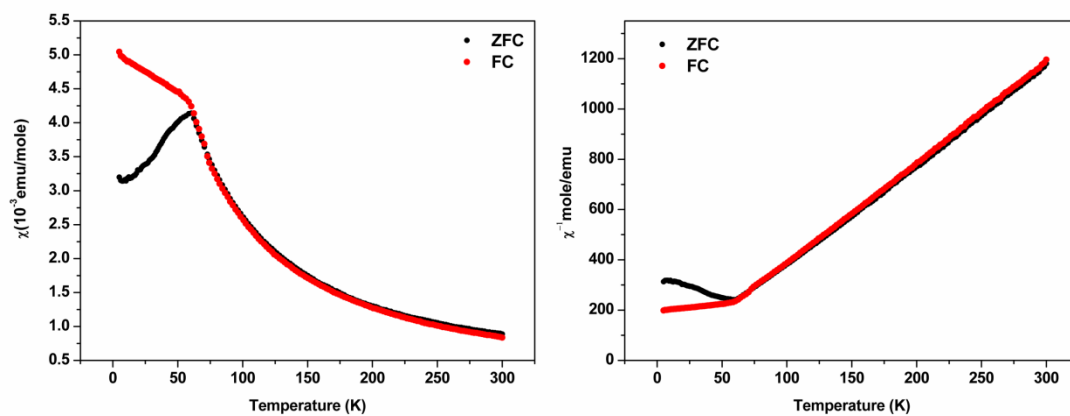


Figure S5c. Molar magnetic susceptibility χ and inverse molar magnetic susceptibility χ^{-1} vs temperature of $\text{BaFe}_{0.82}\text{Bi}_{0.18}\text{O}_{3-\delta}$

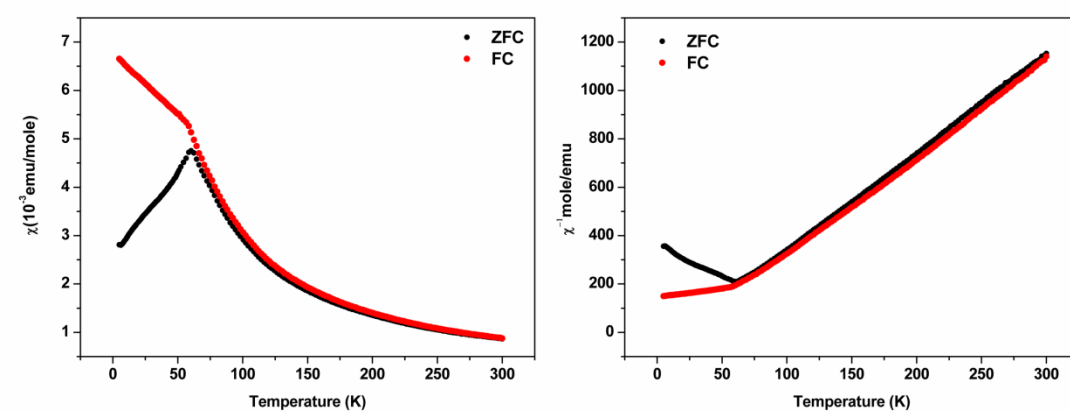


Figure S5d. Molar magnetic susceptibility χ and inverse molar magnetic susceptibility χ^{-1} vs temperature of $\text{BaFe}_{0.79}\text{Bi}_{0.21}\text{O}_{3-\delta}$

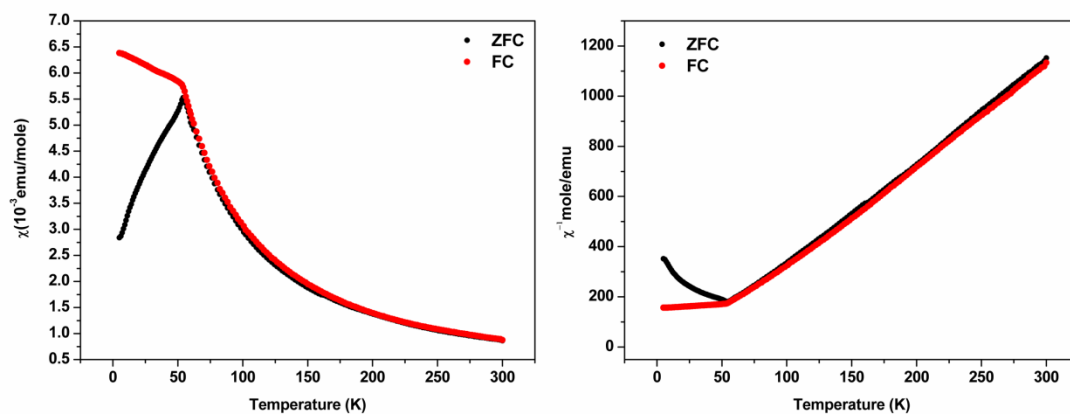


Figure S5e. Molar magnetic susceptibility χ and inverse molar magnetic susceptibility χ^{-1} vs temperature of $\text{BaFe}_{0.73}\text{Bi}_{0.27}\text{O}_{3-\delta}$

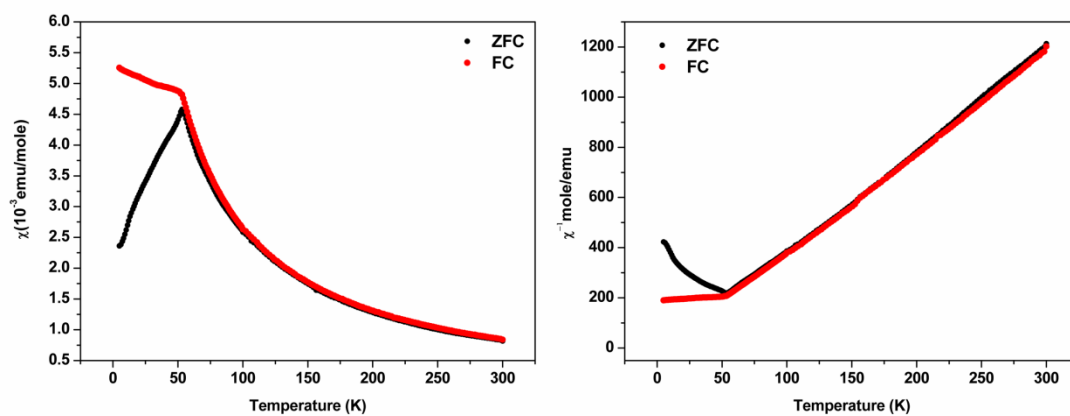


Figure S5f. Molar magnetic susceptibility χ and inverse molar magnetic susceptibility χ^{-1} vs temperature of $\text{BaFe}_{0.70}\text{Bi}_{0.30}\text{O}_{3-\delta}$

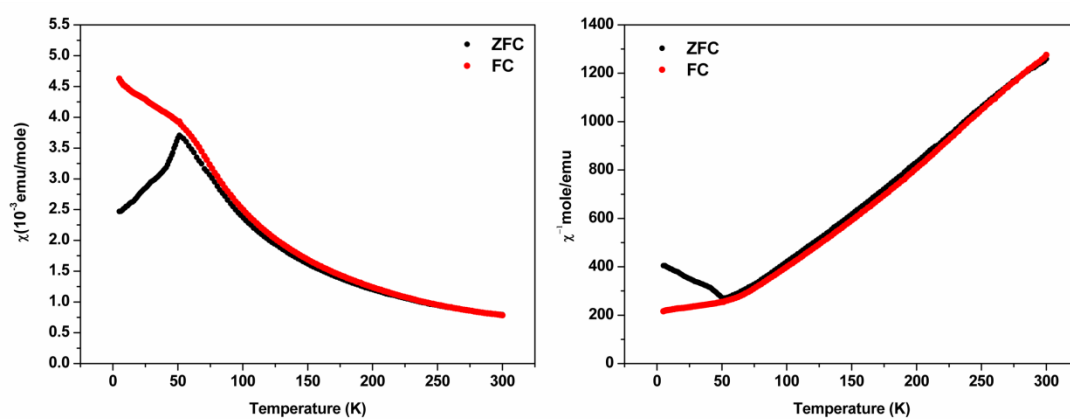


Figure S5g. Molar magnetic susceptibility χ and inverse molar magnetic susceptibility χ^{-1} vs temperature of $\text{BaFe}_{0.65}\text{Bi}_{0.35}\text{O}_{3-\delta}$

6. The ^{57}Fe Mössbauer spectra of $\text{BaFe}_{0.85}\text{Bi}_{0.15}\text{O}_{3-\delta}$ (BFB15).

The ^{57}Fe Mössbauer spectra were obtained using ^{57}Co diffused into rhodium as a source of gamma rays at room temperature.⁸ Absolute velocity calibration was carried out with a Fe foil (25 pm thick); isomer shifts (IS) are reported with reference to Fe.

Table S6. Analysis of the Mössbauer spectra for $\text{BaFe}_{0.85}\text{Bi}_{0.15}\text{O}_{3-\delta}$

| Sample | IS _A /(mm·s ⁻¹) | IS _B /(mm·s ⁻¹) | QS _A /(mm·s ⁻¹) | QS _B /(mm·s ⁻¹) | y(Fe _A)/% | y(Fe _B)/% |
|--------|--|--|--|--|-----------------------|-----------------------|
| BFB3 | 0.359(3) | 0.020(4) | 0.667(3) | 0.507(7) | 75.4(3) | 24.6(3) |

IS: isomer shift; QS: quadrupole splitting; A: Fe³⁺; B: Fe⁴⁺; y: molar fraction of Fe³⁺ or Fe⁴⁺.

7. Rietveld Refinement Details of the neutron diffraction data collected at 55K and 3K for $\text{BaFe}_{0.85}\text{Bi}_{0.15}\text{O}_{3-\delta}$

Table S7. Rietveld Refinement Details of the neutron diffraction data for $\text{BaFe}_{0.85}\text{Bi}_{0.15}\text{O}_{3-\delta}$ in space group *P4/mmm*

| | 55K | 3K |
|-----------------------|---|---|
| Lattice parameters | $a = 4.0723(1)\text{Å}, c = 4.0807(1)\text{Å}$ | $a = 4.0720(1)\text{Å}, c = 4.0804(1)\text{Å}$ |
| Atom | (x,y,z)/ Occupancy/ U _{iso} | (x,y,z)/ Occupancy/ U _{iso} |
| Ba1 | (0.0000, 0.0000, 0.0000)/1.00/0.0077 | (0.0000, 0.0000, 0.0000)/1.00/0.0035 |
| Fe1 | (0.5000, 0.5000, 0.5000)/0.85(1)/0.0172 | (0.5000, 0.5000, 0.5000)/0.85(1)/0.0119 |
| Bi1 | (0.5000, 0.5000, 0.5000)/0.15(1)/0.0172 | (0.5000, 0.5000, 0.5000)/0.15(1)/0.0119 |
| O1 | (0.5000, 0.5000, 0.0000)/0.98(1)/0.0182 | (0.5000, 0.5000, 0.0000)/0.98(1)/0.0134 |
| O2 | (0.5000, 0.0000, 0.5000)/0.93(1)/0.0070 | (0.5000, 0.0000, 0.5000)/0.93(1)/0.0043 |
| R factor ^a | R _{wp} ⁿ = 0.054, R _p ⁿ = 0.037 | R _{wp} ⁿ = 0.056, R _p ⁿ = 0.038 |

^aR_{wp}ⁿ, R_pⁿ are the R factor of the whole patterns and the peaks only for neutron diffraction data, respectively.

References

1. N. Hayashi, T. Yamamoto, H. Kageyama, M. Nishi, Y. Watanabe, T. Kawakami, Y. Matsushita, A. Fujimori and M. Takano, *Angewandte Chemie International Edition*, 2011, **50**, 12547-12550.
2. H. Rietveld, *Journal of Applied Crystallography*, 1969, **2**, 65-71.
3. B. Toby, *Journal of Applied Crystallography*, 2001, **34**, 210-213.
4. U. Gelius, P. F. Hedén, J. Hedman, B. J. Lindberg, R. Manne, R. Nordberg, C. Nordling and K. Siegbahn, *Physica Scripta*, 1970, **2**, 70.
5. W. M. Lau, L. J. Huang, I. Bello, Y. M. Yiu and S. T. Lee, *Journal of Applied Physics*, 1994, **75**, 3385-3391.
6. D. Dissanayake, K. C. C. Kharas, J. H. Lunsford and M. P. Rosynek, *Journal of Catalysis*, 1993, **139**, 652-663.
7. A. B. Christie, J. Lee, I. Sutherland and J. M. Walls, *Applications of Surface Science*, 1983, **15**, 224-237.
8. R. Mössbauer, *Z. Physik*, 1958, **151**, 124-143.